JOURNAL OF APPLIED ELECTROCHEMISTRY 10 (1980) 357–363

The impedance of the Leclanché cell. I. The treatment of experimental data and the behaviour of a typical undischarged cell

S. A. G. R. KARUNATHILAKA, N. A. HAMPSON

Department of Chemistry, University of Technology, Loughborough, Leicestershire, UK

R. LEEK

Department of Electronic and Electrical Engineering, University of Technology, Loughborough, Leicestershire, UK

T. J. SINCLAIR

Procurement Executive, Ministry of Defence, Royal Armament Research and Development Establishment, Fort Halstead, Sevenoaks, Kent, UK

Received 9 June 1979

The impedance spectrum of an undischarged commercial Leclanché cell (Ever Ready type SP11) is presented in the forms of the Sluyters plot and the modified Randles plot. The decomposition of the experimental cell impedances into the component parts has been achieved using a computer. The decomposition process and the component processes representing the overall cell behaviour are described.

List of symbols

R_s	in-phase component of (experimental) electrode impedance
R_t	charge transfer resistance referred to nominal area of Zn ($\Omega\,cm^2$)
$1/(\omega C_s)$	out-of-phase component of (experimental) electrode impedance
ω	angular frequency ($= 2\pi f$)
R_Ω	resistance of electrolyte solution
θ	charge transfer resistance
C_L	double layer capacitance
C_{DL}	double layer capacitance of electrode referred to nominal area of Zn ($\mu F\,cm^{-2}$)
j	$\sqrt{-1}$
σ	Warburg coefficient
D	factor in Equations 1 and 2
$C_s'R_s'$	calculated values of C_s and R_s (first approximation)
$C_s''R_s''$	calculated values of C_s and R_s (refined values taking into account the additional network)
$C_s'''R_s'''$	calculated values of C_s and R_s (refined values taking into account porosity)
θ_x	resistive part of additional series component (parallel connection)
C_x	capacitance part of additional series component (parallel connection)
D'	factor in Equations 6 and 7

1. Introduction

The measurement of impedance over an extended frequency range provides a means of assessing the state-of-charge of electrochemical cells [1]. The Leclanché cell is one of the major commercial primary cells of the contemporary scene. We have considered it of considerable importance, therefore, to be able to measure the frequency response effectively over an extended range and further to be able to interpret the data in terms of the known reactions of the Leclanché cell.

In this paper we present a method for the acquisition of impedance data characteristic of a Leclanché cell using a frequency response analyser.

0021–891X/80/030357–07$02.70/0

The interpretation of the data follows from a computer decomposition of the data using the established frequency response of simple electrode systems based on the zinc electrode. At this point only the undischarged cell behaviour is considered. We wish to emphasize, however, that we are only considering the behaviour of the assembled cell in order to demonstrate the application of the elegant a.c. impedance method to a problem in applied electrochemical technology. In further papers we intend to deal in detail with the kinetics of each electrode process as well as the behaviour of the complete cell as functions of the state-of-charge.

2. Experimental

The cell investigated was an Ever Ready (type SP11) cell available commercially.

The apparatus used for the impedance determinations has been described [2] and incorporates a frequency response analyser (Solatron Type 1170) and a potential controller (Kemitron PC-03). The dry cell was connected between the working and counter electrode terminals of the potential controller and the reference terminal in such a way that the cell voltage was opposed by a voltage of exactly similar magnitude on the potential controller so that there was no net current through the cell. The cell was thus poised at the equilibrium potential. Impedance measurements were made at a series of experimental frequencies in the range 10 kHz to 0.1 MHz the data being presented in the form R_s versus $j/(\omega C_s)$ where R_s and $1/(\omega C_s)$ were the in-phase and out-of-phase components of the impedance. The data points were plotted on an X–Y recorder Bryans 26 000-A3 and printed on a teletype (Data Dynamics ASC 300) with a tape punch facility.

3. Results and discussion

Fig. 1 shows a typical complex plane representation of the impedance data. For this experiment the integration of the signal was performed over a time period 100-fold greater than the optimum minimum as programmed automatically into the frequency response analyser. Attempts to reduce the integration period introduced a considerable amount of scatter into the data. For the general behaviour this was of little consequence, however,

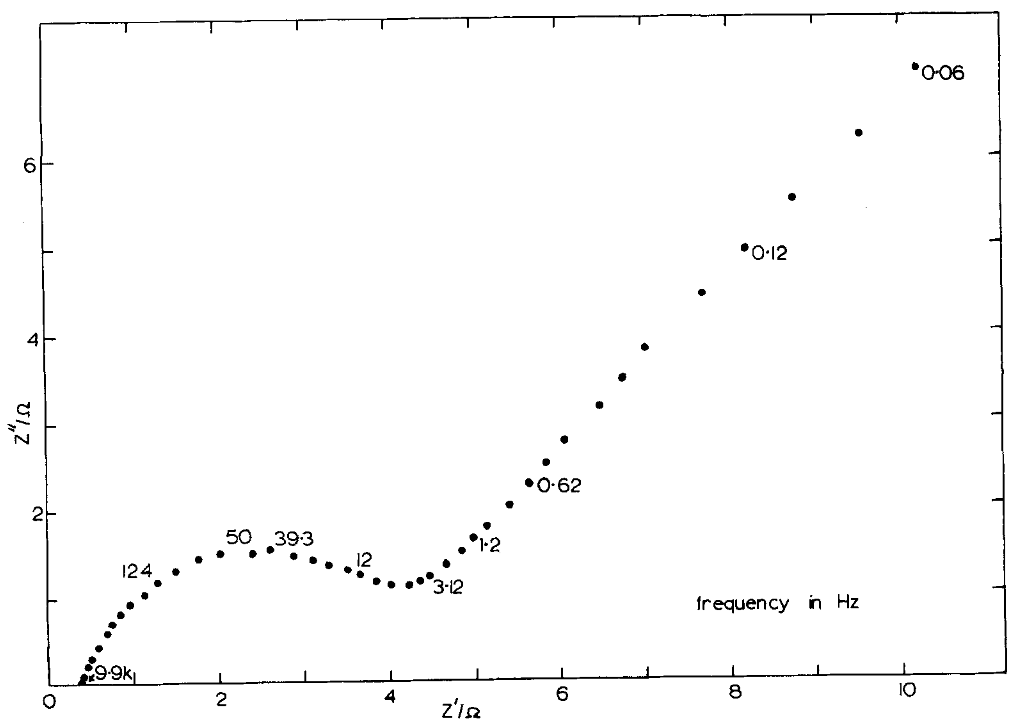

Fig. 1. The frequency response of a Leclanché Cell. Ever Ready SP11, 23° C.

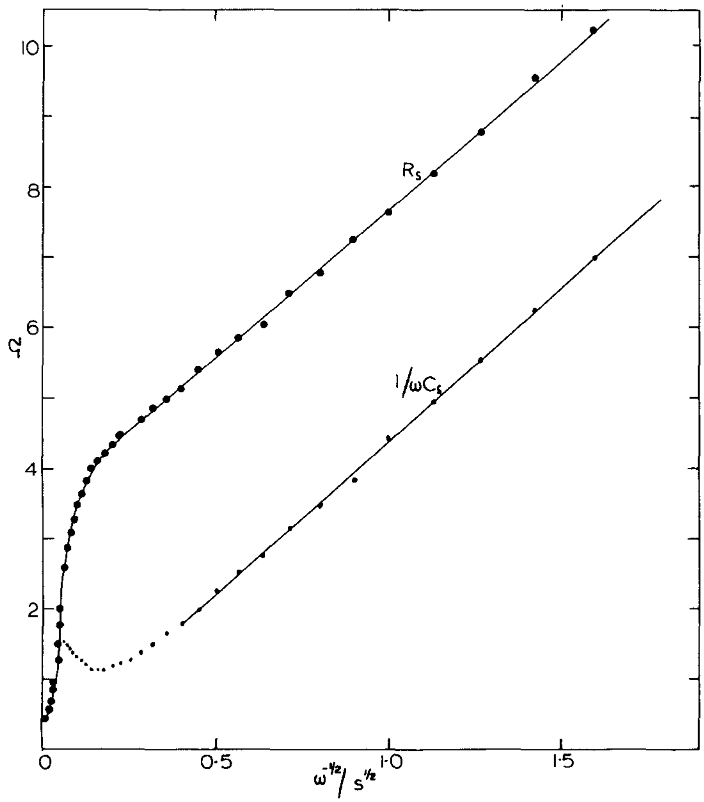

Fig. 2. As for Fig. 1 but R_s and $1/(\omega C_s)$ plotted against $\omega^{-1/2}$, the modified Randles plot.

and, if the data was to be taken out on the punched tape and further processed, the scatter on individual points was troublesome and best avoided by using the long integration time.

Fig. 2 shows the data as plots of R_s and $1/(\omega C_s)$ against $\omega^{-1/2}$. This type of plot was introduced in a slightly simpler form by Randles [3].

Here the relaxation in the in-phase component is due to the double layer and the corresponding hump in the out-of-phase component should extend over two decades of frequency as observed. At lower frequencies the curves become straight lines which are not quite parallel.

3.1. *Decomposition of the impedance data*

3.1.1. Preliminary decomposition. The form of the complex plane plot suggested that the equivalent circuit Fig. 3 would be a first approximation to the electrode analogue. For this [1] the complex representation should be a high frequency semicircle of diameter θ with the centre at $(R_\Omega + \theta/2)$ and $(1/\theta\ C_L)$ as the angular frequency of the maximum point on the semicircle.. This gives the values R_Ω, θ and C_L to a first approximation. The value of the Warburg coefficient $\sigma (W = \sigma\omega^{-1/2} - j\sigma\omega^{-1/2})$ can be obtained from the low frequency slope of either R_s or $1/(\omega C_s)$ in the plots against $\omega^{-1/2}$ since

$$R_s = R_\Omega + \frac{\theta + \sigma\omega^{-1/2}}{(1 + C_L\sigma\omega^{1/2})^2 + \omega^2 C_L^2(\theta + \sigma\omega^{-1/2})^2}$$

$$= R_\Omega + \frac{\theta + \sigma\omega^{1/2}}{D} \tag{1}$$

$$\frac{1}{\omega C_s} = \frac{1}{\omega C_L}\left[1 - \frac{(1 + C_L\sigma\omega^{1/2})}{D}\right] \tag{2}$$

It is clear from Equation 2 that the measured value of C_s should always be greater than C_L.

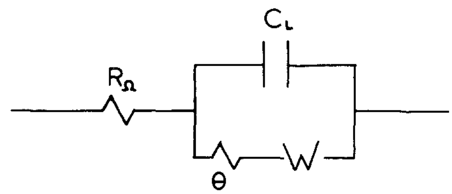

Fig. 3. Equivalent circuit for a simple electrode process with control by charge transfer and diffusion in solution.

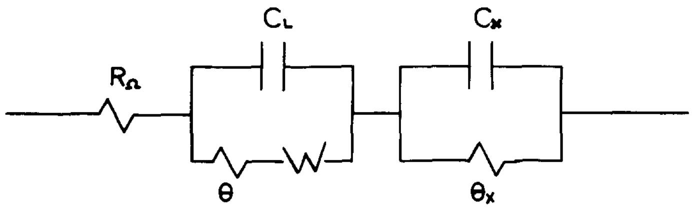

Fig. 4. The cell analogue.

3.2. *Corrections to the approximate analogue*

The complex plane plot (Fig. 1) is a distorted semicircle at high frequencies and furthermore the measured values of C_s are lower than the estimated values of C_L. Refinements to this analogue were introduced by calculating the theoretical behaviour of the circuit, Fig. 3, using the values of θ, C_L and σ obtained from the height of the circle, the intercept at infinite frequency of Fig. 1 (R_Ω) and the slope of the $1/(\omega C_s)$ versus $\omega^{-1/2}$ plot. When this was done, it emerged that the calculated values of $1/(\omega C_s')$ and R_s' were always lower than the observed ones indicating the presence of an additional *C–R* network in series with that of Fig. 3 as shown in Fig. 4.

3.3. *Identification of the additional network*

The differences in the magnitudes $\Delta(1/\omega C) = 1/(\omega C_s) - 1/(\omega C_s')$ and $\Delta R = R_s - R_s'$ were combined to form a vector which was drawn in the complex plane. As the values of ω changed, the vector was found to describe a semicircular locus which may be represented by an equivalent circuit consisting of a capacitance C_x in parallel with a resistance R_x. The calculated refined values of the components R_s'' and C_s'' are now given by

$$R_s'' = R_\Omega + \frac{(\theta + \sigma\omega^{-1/2})}{D} + \frac{\theta_x}{(1 + \omega^2 C_x^2 \theta_x^2)} \tag{3}$$

$$\frac{1}{\omega C_s''} = \frac{1}{\omega C_L}\left[1 - \frac{(1 + C_L \sigma \omega^{1/2})}{D}\right] + \frac{1}{\omega C_x}\left(1 - \frac{1}{1 + \omega^2 C_x^2 \theta_x^2}\right). \tag{4}$$

The values of the individual parameters were next calculated by a method of least squares which was applied separately to Equations 3 and 4. This yielded pairs of values of C_L, C_x, θ and θ_x which agreed to within 2% of each other. The two values obtained for σ, however, differed by 8%.

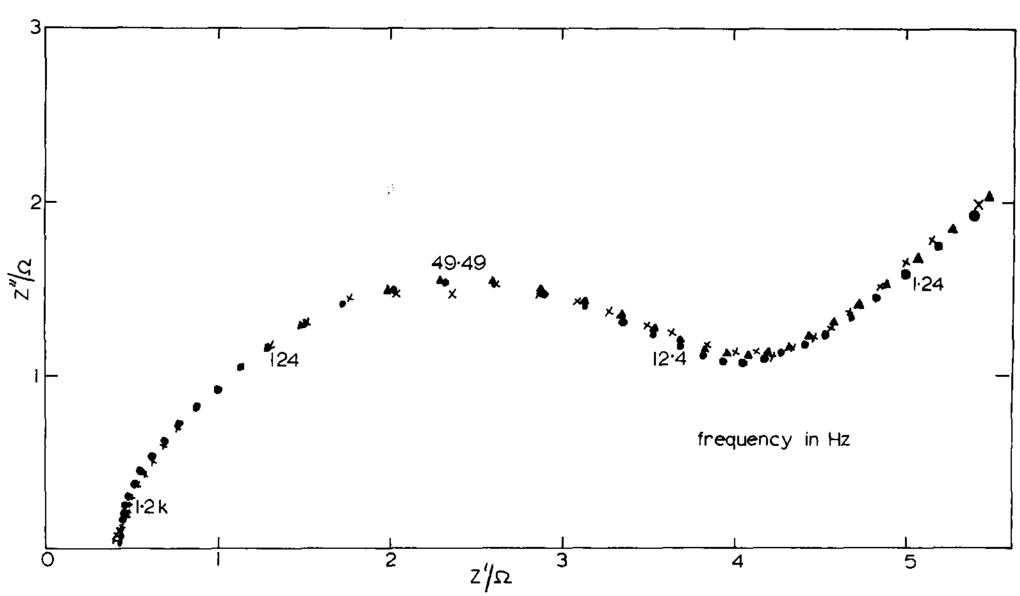

Fig. 5. The data corresponding to the analogue of Fig. 4 in the complex plane compared with the experimental data. X Experimental data; ●, ▲, calculated using the values from Equations 3 and 4, respectively (Table 1).

In Fig. 5 we show the complex plane plot corresponding to this stage; at low frequency the discrepancy between experiment and theory is due to this 8% difference.

3.4. *A refinement to account for porosity*

De Levie [3] in his review emphasizes the effect of a limited roughness on the impedance spectrum. According to this, roughness causes the Warburg impedance to diverge from the 45° slope in the complex plane to a limit of $22\frac{1}{2}°$ for a completely porous electrode (infinite pore length). If pores are very shallow, then the Warburg slope is distorted in the way which we observe here.

Accordingly, we make the modification

$$W = \sigma_R \omega^{-1/2} - j\sigma_C \omega^{-1/2} \tag{5}$$

which, when introduced into Equations 3 and 4, yield two final forms

$$R_s''' = R_\Omega + \frac{(\theta + \sigma_R \omega^{-1/2})}{[(1 + C_L \sigma_C \omega^{1/2})^2 + \omega^2 C_L^2 (\theta + \sigma_R \omega^{-1/2})^2]} + \frac{\theta_x}{1 + \omega^2 C_x^2 \theta_x^2} = R_\Omega + \frac{(\theta + \sigma_R \omega^{-1/2})}{D'} + \frac{\theta_x}{1 + \omega^2 C_x^2 \theta_x^2} \tag{6}$$

$$\frac{1}{\omega C_s'''} = \frac{1}{\omega C_L}\left[1 - \frac{(1 + C_L \sigma_C \omega^{1/2})}{D'}\right] + \frac{1}{\omega C_x}\left(1 - \frac{1}{1 + \omega^2 C_x^2 \theta_x^2}\right) \tag{7}$$

3.5. *The final procedure*

The value of σ_C was fixed at an approximate value by measuring the slope of the capacitance curve of Fig. 2. Values of R_Ω, θ, C_L, θ_x, C_x and σ_R were obtained by applying the method of least squares to Equation 6. The value of σ_R was then substituted into D' in Equation 7 from which values of R_Ω, θ, C_L, θ_x, C_x and σ_C were calculated. This further σ_C was put into Equation 6 and the processes were repeated until no change resulted in σ_R or σ_C by cycling between the two equations. The process was quite rapid and two cycles produced satisfactory values. Typical experimental and calculated values corresponding to the analogue of Fig. 4 with a porosity-modified Warburg coefficient are shown in Fig. 6. Agreement is excellent being < 1% for θ, C_x and θ_x and 2% for C_L between calculations from Equations 6 and 7. The actual values are shown in Table 1 for the analogue with and without modification due to porosity. Results from a nominally similar cell are also shown in Table 1; it is seen that a satisfactory agreement exists between both sets of values.

It should be emphasized that the two sets of results presented here reflect only the behaviour of 'new' undischarged cells; the frequency response

Table 1

Model	R_e*(Ω)	θ(Ω)	C_L(μF)	θ_x(Ω)	C_x(μF)	σ(Ωs$^{-1/2}$)	σ_R(Ωs$^{-1/2}$)	σ_C(Ωs$^{-1/2}$)
$\sigma_R = \sigma_C$; R Equation 3	0.421(19)	2.66(9)	1104(80)	0.56(9)	911(111)	4.09(3)		
$\sigma_R = \sigma_C$; $1/\omega C$ Equation 4		2.69(5)	1091(42)	0.53(5)	909(79)	4.32(1)		
$\sigma_R \neq \sigma_C$; R Equation 6	0.421(19)	2.68(9)	1087(77)	0.55(9)	911(114)		4.085(30)	
$\sigma_R \neq \sigma_C$; $1/\omega C$ Equation 7		2.69(5)	1109(44)	0.55(5)	910(75)			4.328(9)
Cell 2 Equation 6	0.316(9)	2.52(7)	1720(100)	0.75(8)	1302(66)		3.33(2)	
Equation 7		2.42(10)	1975(142)	0.89(11)	1273(112)			3.79(2)

R_t = 84.2(28) Ω cm²
C_{DL} = 34.6(25) μF cm²
* Approximate area of the zinc can = 31 cm²

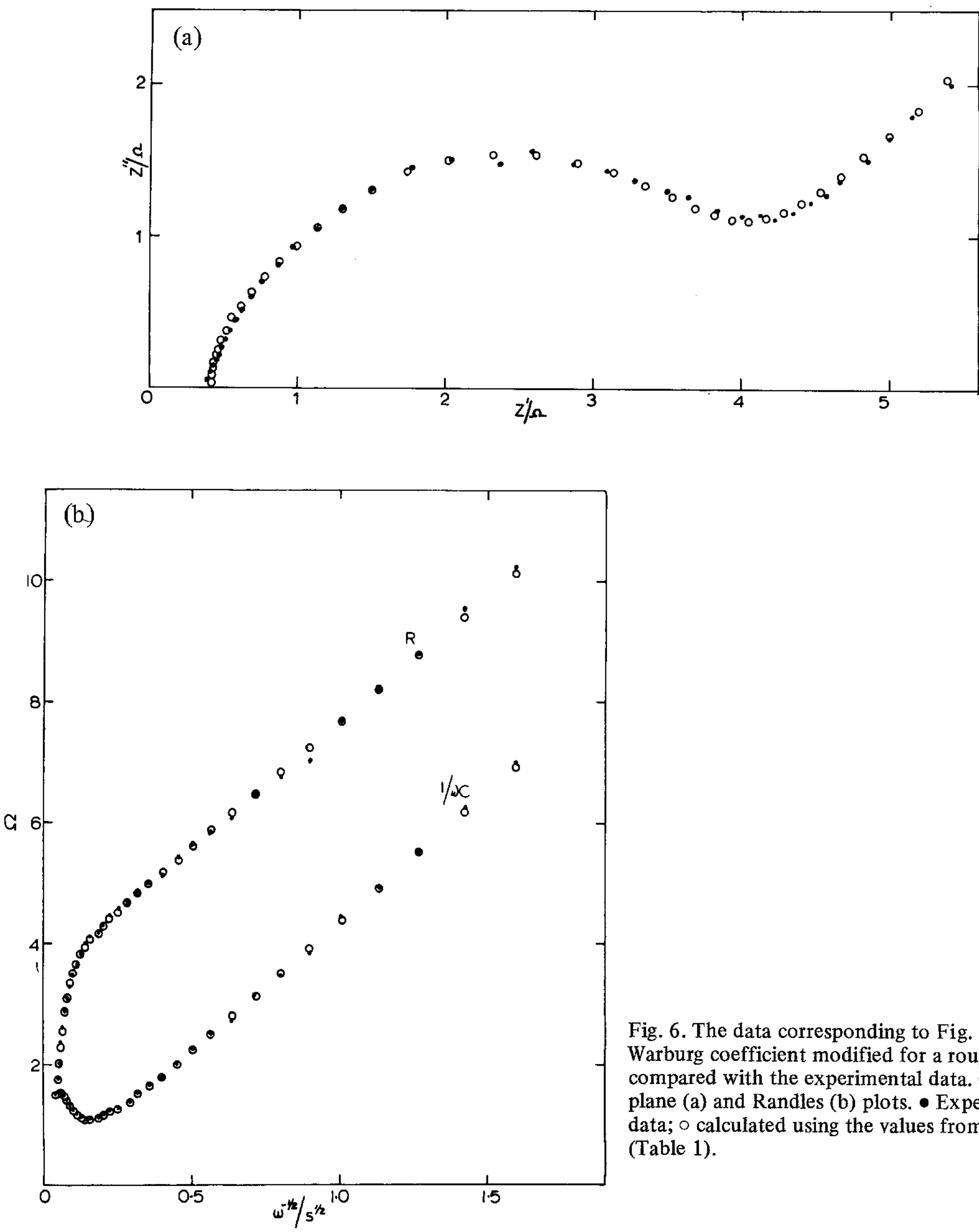

Fig. 6. The data corresponding to Fig. 4 with the Warburg coefficient modified for a rough electrode compared with the experimental data. Complex plane (a) and Randles (b) plots. • Experimental data; ○ calculated using the values from Equation 6 (Table 1).

of undischarged dry cells stored for some time may differ considerably from our present data. These aspects are to be explored in a later paper.

3.6. *The electrochemical interpretation*

The Leclanché cell has a zinc can negative and a complex positive consisting of a carbon rod in contact with finely-divided manganese dioxide. The electrolyte reactions occur across the zinc/ammonium chloride aqueous solution interphase and the manganese dioxide/ammonium chloride aqueous solution interphase. The high surface area of the manganese dioxide ensures that the nominal MnO_2/electrolyte characteristic charge transfer resistance and Warburg coefficient are both small and the corresponding double layer capacitance very large. The zinc electrode charge transfer kinetics and double-layer charging process will be the major observable effects in the electrode impedance spectrum. The frequency-dependent part of the electrode analogue is to be identified with the zinc electrode.

The additional circuit shown in Fig. 4, consisting of a parallel combination of capacitance and resistance whose values are independent of the frequency, is of considerable interest. The size of the capacitance suggests an area of approximately the same magnitude as the zinc electrode and the value of the resistance suggests a relatively poor conductor. The most reasonable interpretation seems to be that this combination arises from the carbon/manganese dioxide junction. The frequency-independence of this combination rules out any electro-activity. At very high frequency, when the zinc double layer effectively obscures the zinc electrode activity, a small difference between measured and calculated frequency response suggests the presence of a small resistance and Warburg component in series with the other two combinations. At present we are unable to isolate this with any degree of certainty.

As a final confirmation that our conclusions are reasonable, we have calculated the double layer capacitance and charge transfer resistance of the zinc using the nominal area of the electrode. These are given in Table 1 and agree with expectations.

4. Conclusions

The following conclusions were reached:

(a) The impedance of an undischarged Leclanché cell can be satisfactorily measured over an extended frequency range.

(b) The experimental data can be deconvoluted to yield a satisfactory electrical analogue for the cell behaviour.

(c) The analogue can be interpreted in terms of control by charge transfer and diffusion at a rough zinc electrode.

(d) The manganese dioxide electrode behaves as a 'counter' electrode of large area.

(e) The geometry of the carbon/manganese dioxide interface produces an effect which may be represented by a combined capacitance and resistance.

Acknowledgement

We thank the Procurement Executive of the Ministry of Defence for financial assistance (to S.A.G.R.K.) and permission to publish this work.

References

[1] N. A. Hampson, S. A. G. R. Karunathilaka and R. Leek, *J. Appl. Electrochem.* **10** (1980) 3.
[2] N. A. Hampson and M. J. Willars, *Surface Tech.* 7 (1978) 247.
[3] R. de Levie, *Adv. Electrochem. Electrochem. Eng.* 6 (1967) 329.